Supplement of

The Flying Laboratory FLab: Development and application of a UAS to measure aerosol particles and trace gases in the lower troposphere

5 Lasse Moormann[1,a], Thomas Böttger[1], Philipp Schuhmann[1], Luis Valero[2,3], Friederike Fachinger[1,a], Frank Drewnick[1,a]

[1] Particle Chemistry Department, Max Planck Institute for Chemistry, 55128 Mainz, Germany
[2] Institute for Atmospheric Physics, Johannes Gutenberg-University, 55128 Mainz, Germany
[3] Institute of Applied Geosciences, Darmstadt University of Technology, 64287 Darmstadt, Germany
10 [a] now at: Multiphase Chemistry Department, Max Planck Institute for Chemistry, 55128 Mainz, Germany

Correspondence to: Frank Drewnick (frank.drewnick@mpic.de)

15 **Table S1: MoLa instruments used for characterization of the FLab.**

Instrument	Measured variables	Time resolution
Aethalometer[a]	Black and brown carbon mass concentration	1 s
CPC[b]	Particle number concentration	1 s
OPC[c]	Particle size distribution based on optical diameter	6 s
O$_3$[d]	Mixing ratio of O$_3$	2 s
LICOR[e]	Mixing ratio of CO$_2$, H$_2$O	1 s
Meteorological station[f]	Wind direction, wind speed, relative humidity, temperature, rain intensity, pressure	1 s
Ceilometer[g]	Altitude-dependent backscatter signal intensity	30 s
FMPS[h]	Particle size distribution based on electrical mobility	6 s

[a]Magee Scientific Aethalometer® Model AE33, Magee Scientific, USA. [b]Condensation Particle Counter Model 3786, TSI, Inc., USA. [c]Optical Particle Counter Model 1.109, Grimm Aerosoltechnik GmbH, Germany. [d]Monitor 205 Dual Beam Ozone Monitor, 2B Technologies, Inc., USA. [e]LI840, LI-COR, Inc., USA. [f]WXT520, Vaisala Oyj, Finland. [g]CHM 15k, Lufft Mess- und Regeltechnik GmbH, Germany. [h]Fast Mobility Particle Sizer Model 3091, TSI, Inc., USA.

20

Table S2: Coefficients for the Hill equations for each variable to calculate the statistical uncertainty of the measured variables from the respective averaging time (in seconds).

Hill equation: $uncertainty\ /\ \% = (base + \frac{max-base}{1+(\frac{xhalf}{averaging\ time})^{rate}}) * 100\%$

| Instrument: variable	base	max	xhalf	rate
AET: black carbon@880nm	4.6664	0.032179	2.8866	1.0122
AET: black carbon@370nm	1.7017	0.019704	2.3234	0.93295
ANE: relative humidity	0.0044786	0.00050038	2.1736	0.78583
ANE: temperature	0.0031714	0.00037684	2.0814	0.79232
ANE: wind speed	0.056469	0.00020911	1.3282	0.58095
CBO: CO$_2$ mixing ratio	0.0039588	0.0010941	7.9264	0.98681
CPC: particle number conc.	0.02681	0.0033615	37.358	0.26378
OPC: particle number conc.	0.17411	0.019143	2.188	0.61314
OPC: PM$_1$	0.19538	0.018385	2.3192	0.62145
OPC: PM$_{2.5}$	0.83355	0.0014132	0.67953	0.52631
OZN: O$_3$ mixing ratio	0.060544	0.013247	7.0617	0.67567
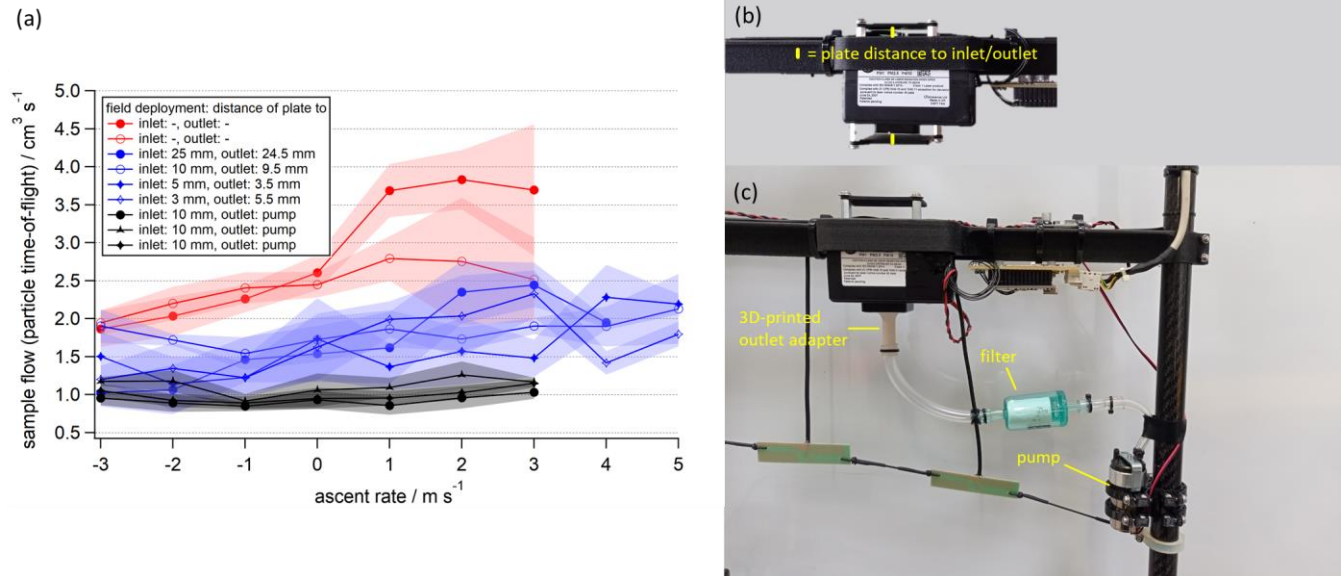
Figure S1: The distance between the plate and the inlet/outlet of the OPC affects the sample flow differently with changing vertical velocity of the FLab (a). Setup of the plates in front of the inlet and behind the outlet of the OPC (b) and setup with an external pump (c) replacing the fan (Bezantakos et al., 2021). Lines between markers are for orientation and are not intended to indicate a 30 relationship.
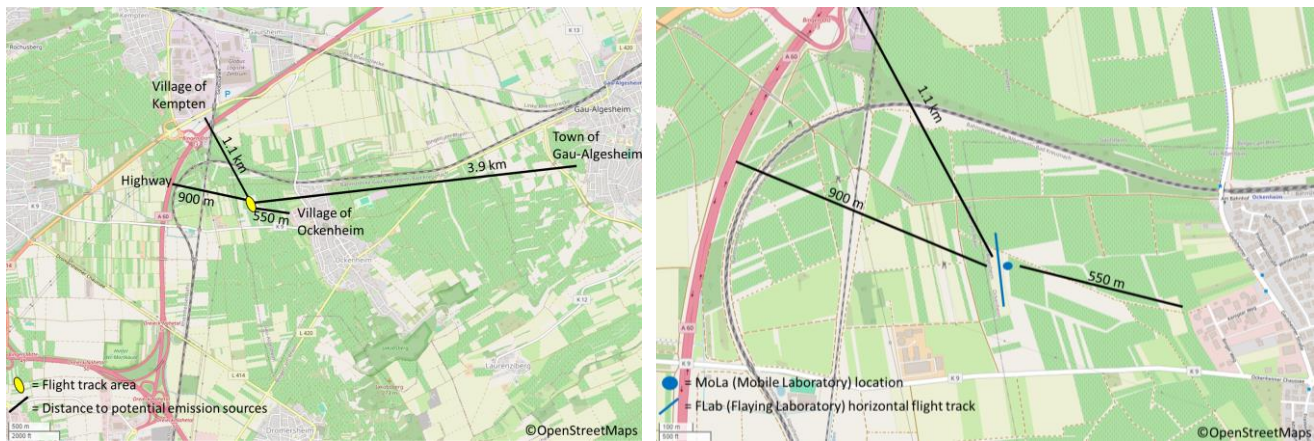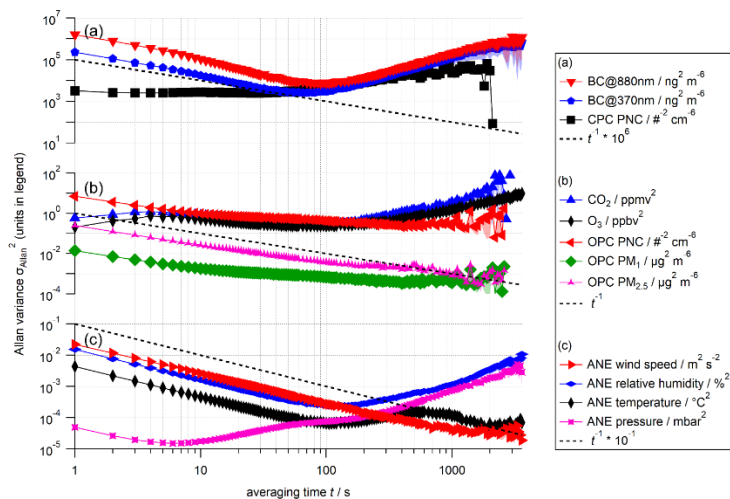

Figure S2: Measurement site near Ockenheim used for the horizontal and vertical characterization flights in Sections 3.2 and 3.3 as well as for the field experiment in Section 4.1.

3

Figure S3: Allan variance of the measured quantities of the FLab instruments as a function of averaging time, presented in three sub-panels (a-c) for clarity. Markers show the mean over the time series, while the standard error is shown as a shaded area (Röder et al., 2023). t^{-1} **represents the slope of the statistically expected Allan variance.**
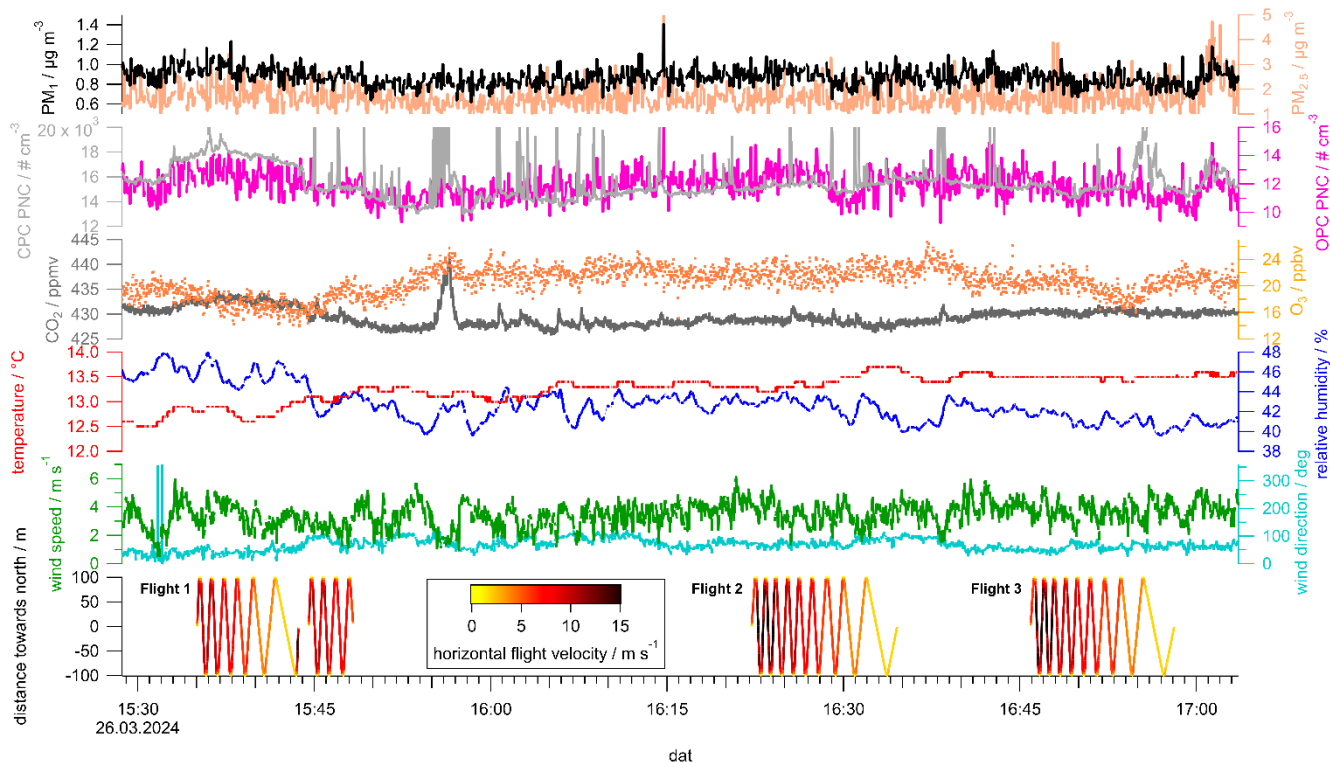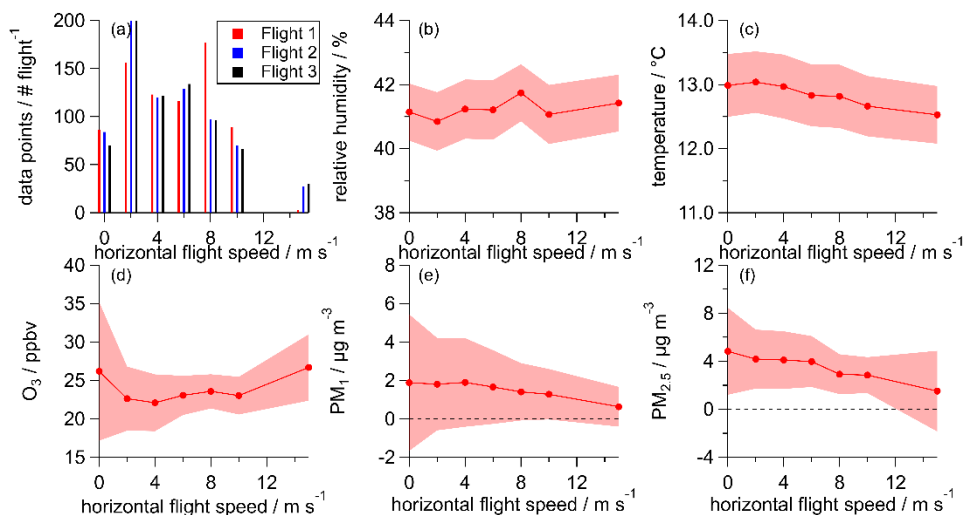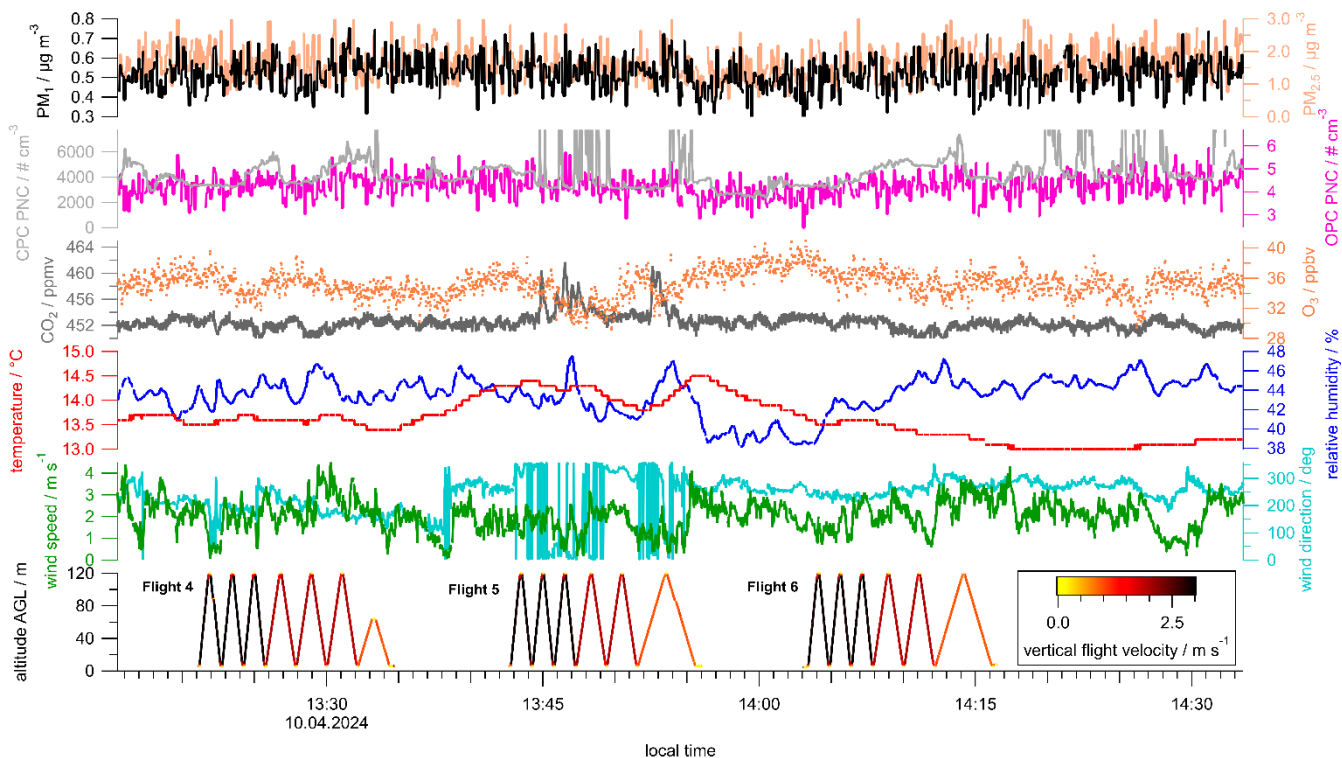

Figure S4: Time series of various quantities measured by MoLa (top five panels) on 26 March 2024, showing a change in air masses and pollutants during flight F1 and stable conditions during flights F2 and F3 (bottom panel).
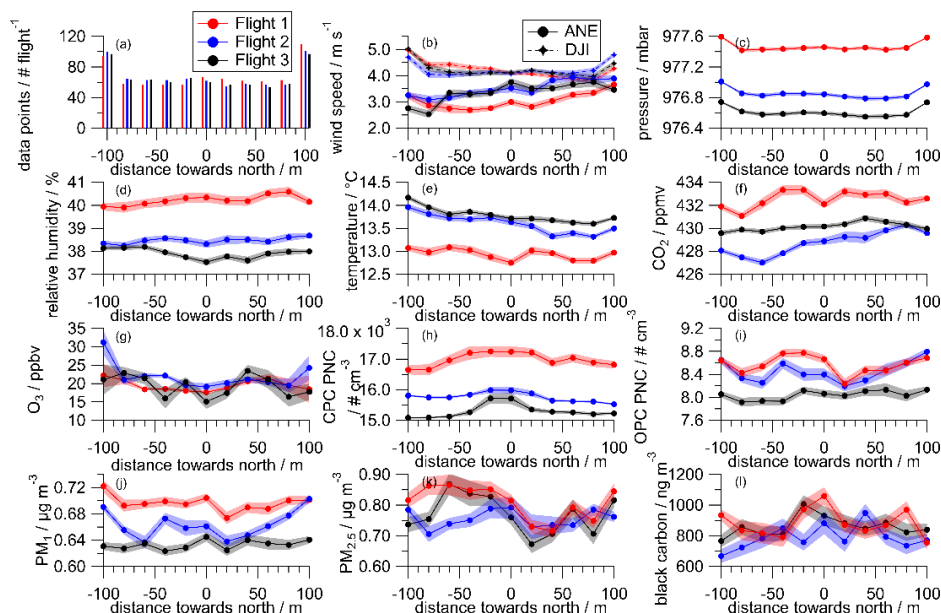
Figure S5: Number of data points collected by FLab (a) for horizontal flight 1 (red), flight 2 (blue) and flight 3 (black) with: wind speed determined by ANE (b, dots) and DJI (b, diamonds), pressure (c), relative humidity (d), temperature (e), CO_2 (f) and O_3 mixing ratios (g), CPC and OPC particle number concentrations (h and i), particulate matter PM_1 (j) and $PM_{2.5}$ (k) determined from the OPC data, and black carbon mass concentrations (l). The shaded areas indicate the standard error.

Figure S6: Effect of horizontal flight velocity on measured variables. Number of data points per velocity setting (a) during Flight 1 (red), Flight 2 (blue) or Flight 3 (black) and average flight speed dependence for relative humidity (b), temperature (c), O_3 mixing ratio (d), and particulate matter PM_1 (e) and $PM_{2.5}$ (f) determined from the OPC. The shaded areas show the uncertainty determined as described in Sect. 3.2.

Figure S7: Time series of various quantities measured by MoLa (top five panels) on 10 April 2024, showing stable environmental conditions during flights F4 and F6 and peaks in small particle concentrations and CO₂ during flight F5 (altitude derived from FLab measurements, bottom panel).
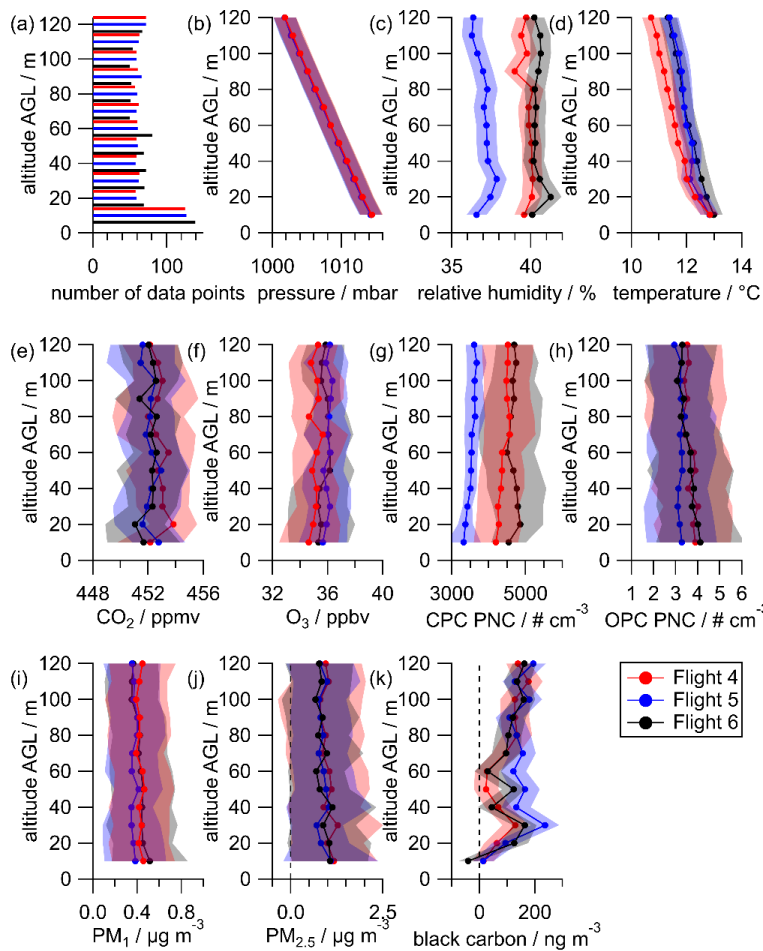
Figure S8: Vertical profiles were measured with FLab during flights F4 (red), F5 (blue) and F6 (black). Averages for 10 m increments were calculated from the number of data points presented in (a) and are shown for the following variables: pressure (b), relative humidity (c), temperature (d), CO_2 (e) and O_3 mixing ratios (f), particle number concentration measured with CPC (g) and OPC (h), particulate matter PM_1 (i) and $PM_{2.5}$ (j), and black carbon concentration (k). The shaded areas show the combined standard error and instrumental uncertainty within the 10 m altitude AGL increments.
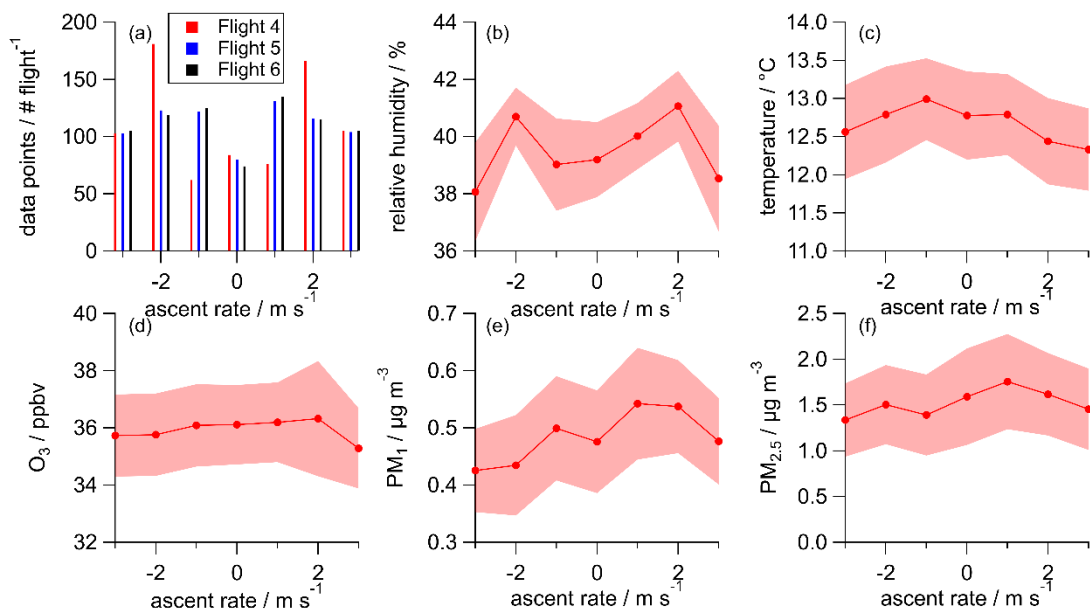
Figure S9: During flight 4 (red), flight 5 (blue) and flight 6 (black) the number of data points (a) of the following atmospheric variables measured with FLab seem to be largely unaffected by its ascent/descent rate: relative humidity (b), temperature (c), O_3 mixing ratio (d) and particle mass concentrations PM_1 (e) and $PM_{2.5}$ (f) measured with OPC. Error bars show the uncertainty (determined as described in Sect. 3.2) within the 1 m s^{-1} increments. The lines between the markers are for orientation only and are not intended to indicate a relationship.
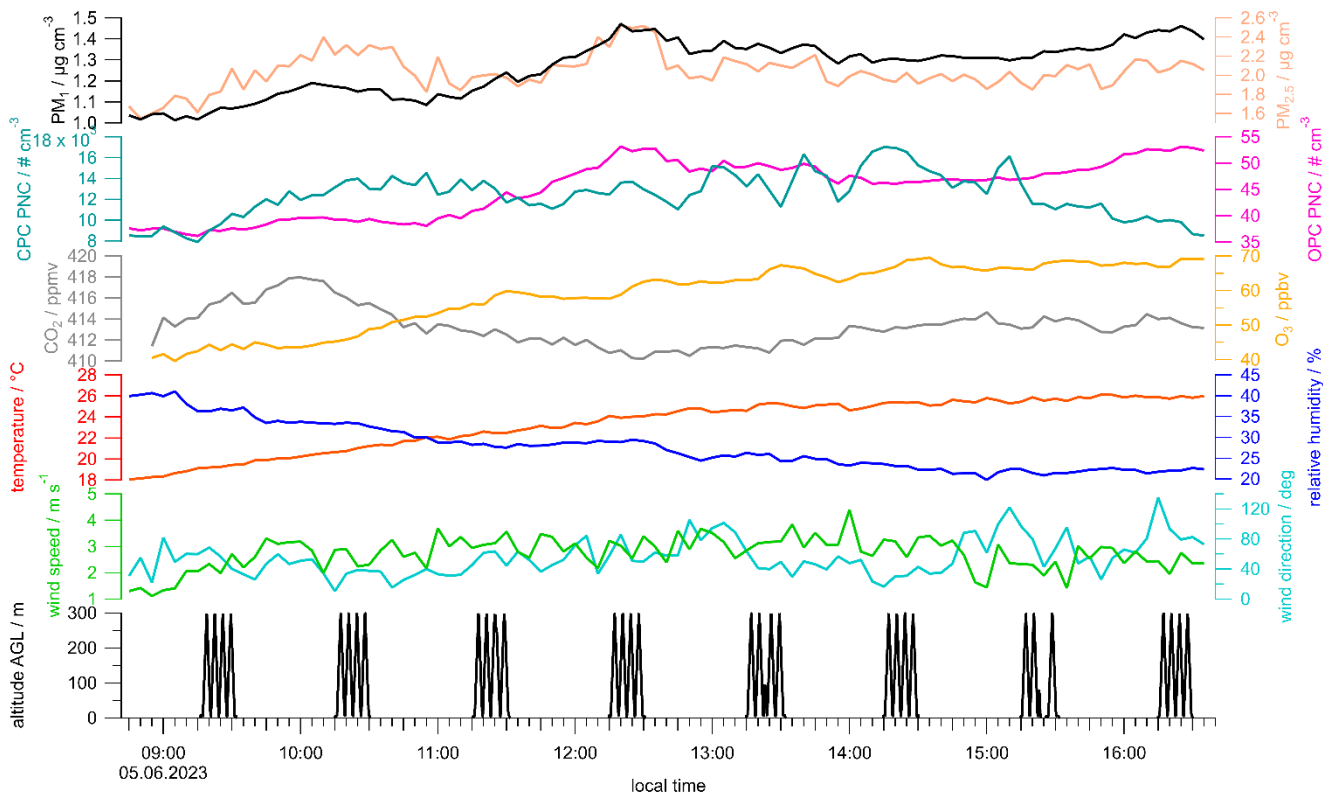
75   **Figure S10: Time series of variables measured with MoLa on 5 June 2023 at a rural site in Ockenheim show an increase in particle occurrence at 9:15 and in the afternoon, while O₃ and air temperature increase and CO₂ and relative humidity decrease during the day. No air mass changes due to changes in wind direction or emission sources were observed at MoLa. Time series of measured variables were averaged to 5 minutes.**
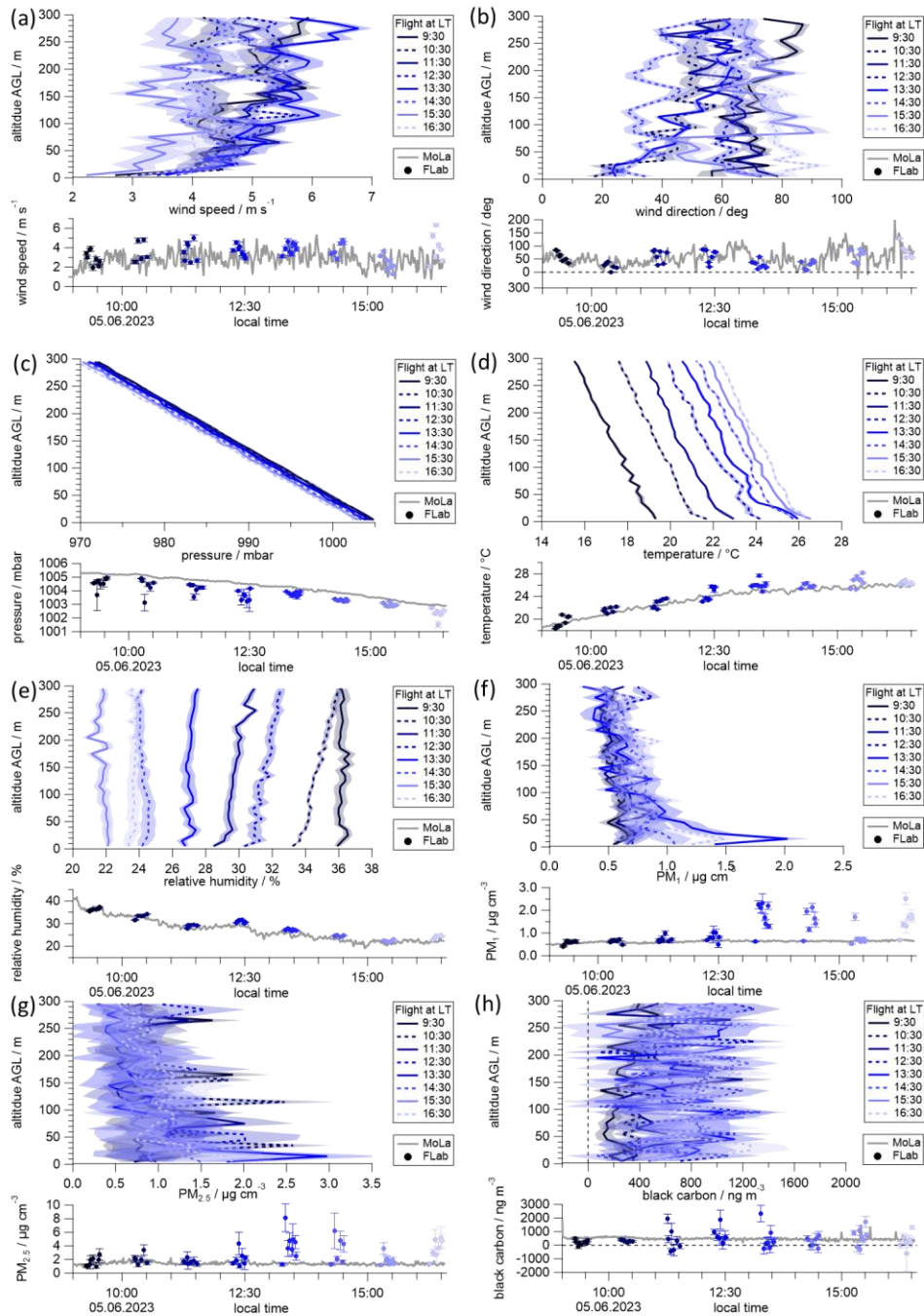
Figure S11: Vertical profiles measured with FLab on 5 June 2023 (upper panels of the subfigures) showing trends of pressure (a), temperature (b), relative humidity (c), wind direction (d) and wind speed (e), and particle mass concentrations for PM_1 (f), $PM_{2.5}$ (g), and black carbon (h). Comparison measurements between MoLa (gray) and FLab (blueish) are performed when FLab was hovering below 10 m AGL next to MoLa (lower panels of subfigures).

80
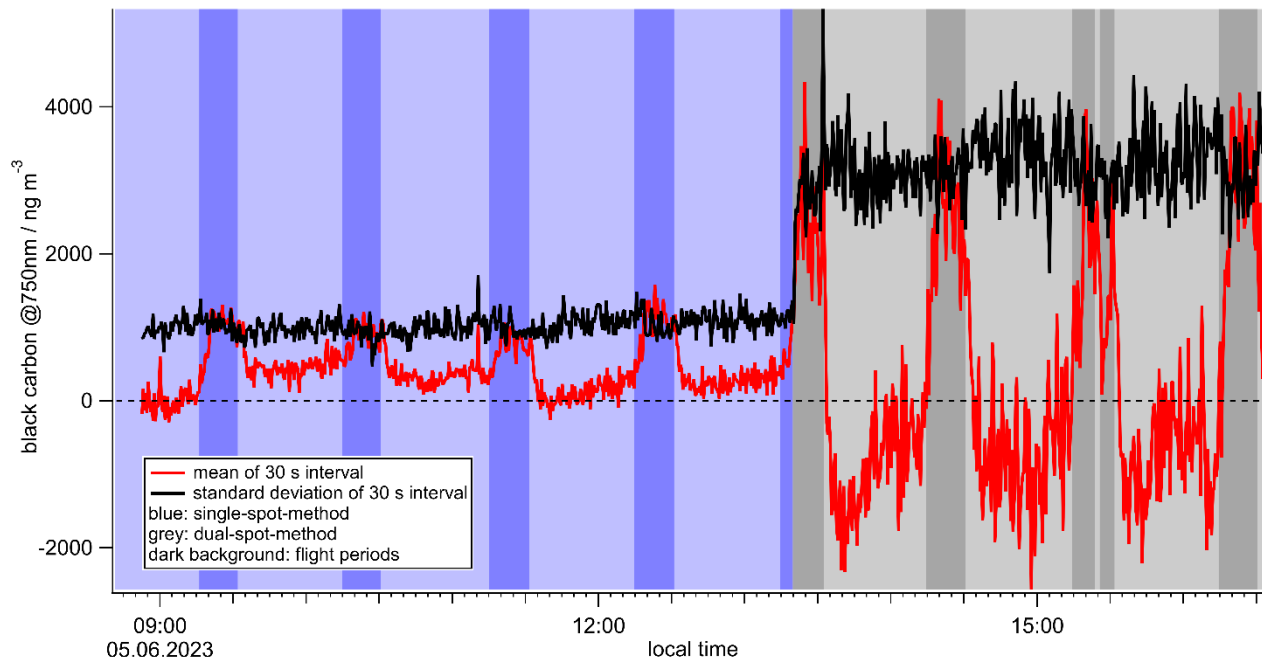
Figure S12: Time series of the black carbon concentration measured with the MA200 Aethalometer showing differences between single-spot (blue) and dual-spot (gray) modes as well as between flight (dark) and nonflight (light) periods.
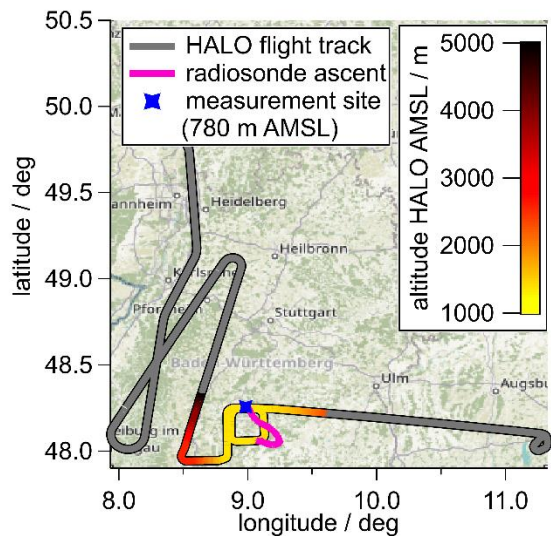
Figure S13: Flight tracks of the radiosonde (pink) and the HALO aircraft (yellow to red below 5000 m and gray > 5000 m above mean sea level, AMSL) during the overflight of the BISTUM23 site at 778 m AMSL (blue), which was the base for the MoLa and FLab measurements and the launch site of the radiosonde.

11

S3: Comparison of radiosonde and FLab data in the lowest 500 m AGL

To assess the comparability of radiosonde and FLab data, three additional measurements with quasi-simultaneous radiosonde
launches and FLab flights are presented in Figure S14 in addition to the radiosonde data shown in Fig. 8. The radiosondes
were launched from the site described in Sect. 4.2 on different days after noon. All radiosondes carried a brand new, freshly
unpacked RS41-sensor (Vaisala Oyj, Finland). The radiosondes provide data such as relative humidity, temperature, horizontal
wind speed and direction, and position, which was used to calculate the distance to the reference station MoLa (Jost et al., in
preparation for AMT). Shaded areas show the uncertainty resulting from the instrument uncertainty and the variation within
the 50 m altitude increments.

In contrast to Figure 8, the difference in relative humidity between the FLab and radiosonde measurements varies widely, but
is usually within the uncertainty range, with no systematic positive or negative offset between the two. Together with the
observation of almost cloud-free conditions on 10 Aug 2023, but a relative humidity measured with the radiosonde of about
90% at 500 m AGL (Fig. 8), this suggests that the sensor used in the flyby scenario shown in Figure 8 may have malfunctioned.
Temperature measurements at altitudes > 50 m AGL are in good agreement for all measurements, whereas the respective
preparation ground before launch may influence the temperature measurement in lowest altitudes (radiosondes prepared on a
tarpaulin, FLab on wooden planks on grassland).

The agreement of wind speed and direction measurements between the two platforms is highly dependent on weather
conditions. In low wind conditions (wind speed < 5 m s^{-1}), the radiosonde ascends almost vertically. The sensor mounted 50 m
below the balloon swings loosely horizontally after the abrupt launch, as indicated by the oscillating distance to MoLa
(Fig. S14a and c). Furthermore, the wind has a direct influence on the motion of the balloon, which is transmitted to the payload
(where the position measurement takes place) via the 50 m long tether. This results in a motion of the payload which is driven
by the wind conditions almost 50 m above its own position. Both effects cause a difference in the radiosonde wind measurement
compared to that of the FLab. Under windy conditions (wind speed > 5 m s^{-1}), FLab and the radiosonde are in much better
agreement at low altitudes (Fig. S14 b), however, a slight difference in the horizontal wind speed measured on both platforms
is observed above 300 m AGL. At this altitude, the difference is probably due to the increasing distance between the radiosonde
and FLab, while the 10° wind direction difference is not affected by the increasing distance. A more detailed analysis of these
differences is not possible due to the lack of detailed information on the processing of the radiosonde data.

In summary, the quality of the radiosonde humidity data is highly dependent on the individual sensor, while ground preparation
conditions can also slightly affect humidity and temperature measurements, however, differences above 50 m AGL are
typically negligible. Windy launch conditions allow a better estimation of wind speed with the radiosonde just above ground,
but may cause a greater difference between the balloon-borne and FLab measurements at higher altitudes due to the increasing
horizontal distance between the two platforms. Since wind speed during the launch on 10 August 2023 was rather low (Fig. 8),
this explains the discrepancy between FLab and radiosonde measurements during this flight.
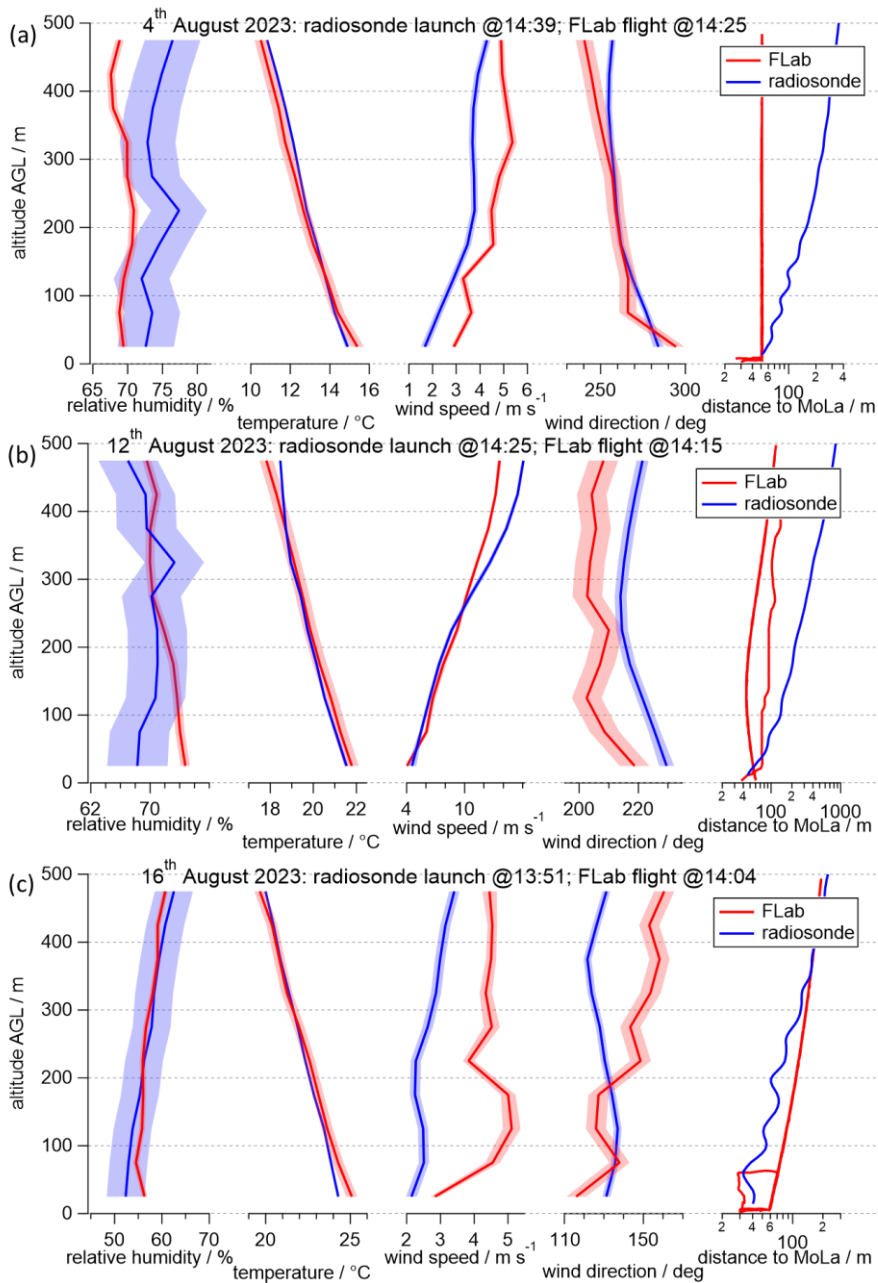
Figure S14: Meteorological data (relative humidity, temperature, and horizontal wind speed and direction) were measured with radiosondes (blue) and FLab (red) up to 500 m AGL during the BISTUM23 campaign. The distance between the platforms and the stationary MoLa ground station reflects the oscillating flight behavior of the radiosonde (hanging about 50 m below the balloon) after launch.

13

References

Bezantakos, S., Costi, M., Barmpounis, K., Antoniou, P., Vouterakos, P., Keleshis, C., Sciare, J., and Biskos, G.: Qualification of the Alphasense optical particle counter for inline air quality monitoring, Aerosol Science and Technology, 55, 361-370, https://doi.org/10.1080/02786826.2020.1864276, 2021.

Röder, L. L., Ort, L. M., Lelieveld, J., and Fischer, H.: Determination of Temporal Stability and Instrument Performance of an airborne QCLAS via Allan-Werle-plots, https://doi.org/10.21203/rs.3.rs-3619758/v1, 2023.